Materials Science-Poland, 40(3), 2022, pp. 42-63
http://www.materialsscience.pwr.wroc.pl/
DOI: 10.2478/msp-2022-0033

Hardfacing of mild steel with wear-resistant Ni-based powders containing tungsten carbide particles using powder plasma transferred arc welding technology

Augustine Nana Sekyi Appiah[1,*], Oktawian Bialas[2], Marcin Żuk[3], Artur Czupryński[3], David Konadu Sasu[4], Marcin Adamiak[1]

[1]Materials Research Laboratory, Faculty of Mechanical Engineering, Silesian University of Technology, 18A Konarskiego Street, 44-100 Gliwice, Poland

[2]Department of Engineering Materials and Biomaterials, Faculty of Mechanical Engineering, Silesian University of Technology, 18A Konarskiego Street, 44-100 Gliwice, Poland

[3]Welding Department, Faculty of Mechanical Engineering, Silesian University of Technology, 18A Konarskiego Street, 44-100 Gliwice, Poland

[4]Department of Materials Engineering, College of Engineering, PMB UPO, KNUST Kumasi, Ghana

This study explores the use of powder plasma transferred arc welding (PPTAW) as a surface layer deposition technology to form hardfaced coatings to improve upon the wear resistance of mild steel. Hardfaced layers were prepared using the PPTAW process with two different wear-resistant powders: PG 6503 (NiSiB + 60% WC) and PE 8214 (NiCrSiB + 45% WC). By varying the PPTAW process parameters of plasma gas flow rate (PGFR) and plasma arc current, hardfaced layers were prepared. Microscopic examinations, penetration tests, hardness tests, and abrasive wear resistance tests were carried out on the prepared samples. Hardfacings prepared with PG 6503 had a hardness of 46.3–48.3 HRC, while those prepared with PE 8214 had a hardness of 52.7–58.3 HRC. The microhardness of the matrix material was in the range of 573.3–893.0 HV, while that of the carbides was in the range of 2128.7–2436.3 HV. The abrasive wear resistance of the mild steel was improved after deposition of hardfaced layers by up to 5.7 times that of abrasion-resistant heat-treated steel, Hardox 400, having a nominal hardness of approximately 400 HV. The hardness and wear resistance were increased upon addition of Cr as an alloying element. Increasing the PGFR increased the hardness and wear resistance of the hardfacings, as well as increasing the number of surface cracks. Increasing the plasma transferred arc (PTA) current resulted in hardfacings with fewer cracks but lowered the wear resistance.

Keywords: *microhardness, microstructure, mechanical properties, scanning electron microscopy, dilution, heat affected zone*

1. Introduction

Metallic materials in use tend to degrade with time and eventually lose their usefulness. Conditions such as corrosion, creep, and wear contribute to the failure of these materials. Studies have shown that most of these failure mechanisms originate from the surface of the material, and an effective way of solving such problems is using surface treatment technologies such as physical vapor deposition (PVD), chemical vapor deposition (CVD), thermal spraying, laser cladding (LC), and plasma transferred arc welding (PTAW) [1]. Surface engineering technologies have had a widespread use in several engineering disciplines, including construction, power, automotive, etc. [2]. Deposition technologies are being used to develop advanced functional properties that the required substrate surfaces can be imbibed with, and some examples of these properties are corrosion resistance, wear resistance, and mechanical, magnetic, electrical, and optical properties [3]. All types of materials, including metals, polymers, ceramics, and composites, can be deposited onto similar or dissimilar materials. These technologies also allow for the formation of coatings of advanced engineering materials, metamaterials, multicomponent deposits, graded deposits, etc. For high temperature industrial applications, Kołodziejczak et al. [4]

* E-mail: augustine.appiah@polsl.pl

studied the oxide and corrosion resistance of laser cladded Ni-Cr alloy with 1% rhenium. The resulting clads showed no evidence of defects, amidst varying dilution levels.

Deposition technologies are used to alter the chemical and physical properties as well as the morphology of the surface of the substrate. In a study by Kołodziejczak et al. [5], cold metal transfer (CMT) technology was used to deposit protective layers consisting of Stellit 6, Alloy 33, Inconel 625, and Inconel 718 on a 16Mo3 steel substrate. Results from this study indicated that the CMT technique produced layers with superior properties, influenced by the low dilution associated with this technique. Techniques for the deposition of nanocrystalline coatings to improve on the mechanical properties of metals have also been explored [6]. Górka et al. [7] investigated the wear resistance of Fe-Cr-Nb-B deposited on S355 steel using manual metal arc (MMA) technology. The study reported increased wear resistance and hardness after remelting of the Fe-Cr-Nb on the structural steel substrate.

Surface treatment provides strategic ways of saving materials as well as aids in the design of components with desirable surface properties. This serves as a cheaper alternative to using conventional materials to serve similar surface treatment purposes in large scale production. PTAW, however, has been identified as an effective technology that can be used to overcome the surface treatment limitations, such as dilution and poor adhesion, which characterize other hardfacing technologies [8]. The PTAW technique has been in application since 1962, a time when the technology was used to modify materials' surfaces by producing overlays [9]. In this technique, a plasma arc is created and confined around an electrode (e.g., a tungsten [W] electrode), which is placed in a torch and mostly used as the cathode. The powder to be deposited is injected into the plasma in the presence of a shielding gas onto the substrate or workpiece, which is the anode. This shielding gas helps to prevent melting of the powder particles against oxidation [10]. Plasma arc has a high ionization, and this enables it to be fine-tuned to obtain desired results with regard to penetration and dilution. PTAW results in surface overlays of remarkably high quality [11]. Relative to other methods of surface layers deposition, PTAW has many advantages. The PTAW technique results in an improved adhesion between the overlays and the substrate. The energy flux associated with PTAW has a high stability. This technique has a relative higher melting efficiency [12]. The cost associated with PTAW welding implementation is lower while maintaining a higher efficiency [13]. The filler material for PTAW could either be in the form of a wire (called plasma arc welding [PAW]) or powders (called powder plasma transferred arc welding [PPTAW]). However, the powders are widely used in application, making heat demands for melting low [14]. The properties of the overlays produced from PPTAW depend primarily on the powder material used. However, the process parameters also contribute to the quality of the overlays. The most significant process parameters for wear-resistant applications are the plasma gas flow rate (PGFR) and plasma arc current [15]. Industrial applications of PPTAW technology have increased over the years, due to its compatibility of use with different powder materials. Most industrial uses of this technology are for abrasive resistance, corrosion resistance, and wear resistance. Some advanced industrial applications of PPTAW include the production of self-lubricating surfaces, and high temperature wear resistance [16]. PPTAW is used to address materials' failure challenges in industries such as marine, ore mining, petrochemical, oil drilling, steel manufacturing, power generation, etc. [17, 18].

This study explores the potential of PPTAW technology, as an easy-to-use technology for hardfacing parts and components with geometries either simple or complex, by using the powders of wear-resistant Ni-based materials reinforced with WC particles to prepare hardfaced layers to improve the wear resistance of a mild steel plate. The paper also investigates the effects of the process parameters on the microstructure, mechanical properties, and dilution associated with this technique.

Table 1. PTAW parameters for sample preparation

Coating/sample ID	Powder used	Current (A)	Travel speed, V (mm/s)	PGFR (l/min)
PG-1	PG 6503	110	1.3	1.0
PG-2	PG 6503	110	1.3	1.2
PG-3	PG 6503	150	1.3	1.2
PG-4	PG 6503	110	1.3	1.5
PE-5	PE 8214	110	1.3	1.0
PE-6	PE 8214	110	1.3	1.2
PE-7	PE 8214	150	1.3	1.2
PE-8	PE 8214	110	1.3	1.5

PGFR, plasma gas flow rate; PTAW, plasma transferred arc welding

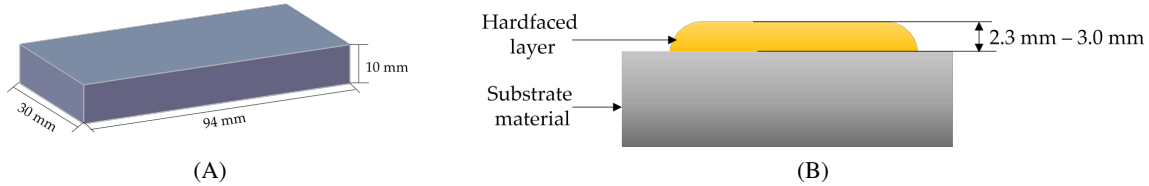

Fig. 1. Schematic diagrams showing the dimensions of the prepared samples. **(A)** Dimensions of the prepared mild steel plate to be used as a substrate material. **(B)** Cross-section of the final material after deposition of the hardfaced layer onto the substrate material, showing the range of thickness of the hardfaced layers for the various samples

2. Materials and methodology

2.1. Sample preparation

The main process for preparing the samples used in this work was the PPTAW process. The sample preparation was carried out using the EuTronic© Gap 3511 DC synergic system (Eutectic Castolin, Chrášťany, Czech Republic) at the Castolin Eutectic© workshop in Gliwice, Poland. Argon 5.0 (99.999%) acc. ISO 14175-I1: 2009 was used as plasma; argon/hydrogen 5% H_2, Ar (welding mixture ISO 14175-R1-ArH-5) was used as the shielding and carrier gas; and a thermal efficiency coefficient of k = 0.6 was used for the plasma transferred arc (PTA). The electrode used was tungsten (WS-2), with a diameter of 4 mm and a plasma nozzle size of 3 mm. The PPTAW process parameters that were considered for preparing various samples were PGFR, plasma arc current, and torch travel speed. Two distinct groups of samples were prepared using two different wear-resistant powders for the PPTAW hardfaced layers. The base/substrate material used was a mild steel plate, grade EN S355, with dimensions 94 mm × 30 mm × 10 mm, as shown in Figure 1A. The powders, PG 6503 and PE 8214, were obtained from Castolin Eutectic©. PG 6503 consisted of the NiSiB matrix with 60% WC and PE 8214 consisted of the NiCrSiB matrix with 45% WC. Eight samples were prepared in total; four for each powder, with varying PTAW process parameters. To obtain the desired microstructure and mechanical properties of a hardfaced layer, selection of optimal PPTAW process parameters is a key step. The most reliable hardfaced layers are those configured and prepared to have the least surface defects, high rate of deposition, and less distortion, as well as low dilution [19]. The PPTAW process parameters – PGFR and plasma arc current – were varied to obtain information on their effects on the structure and properties of the hardfaced layers. Additionally, variation of these process parameters provides control over the PPTAW process for easier reproducibility of hardfaced layers with superior wear-resistant properties. The parameters for preparing the layers are given in Table 1. The thickness of the

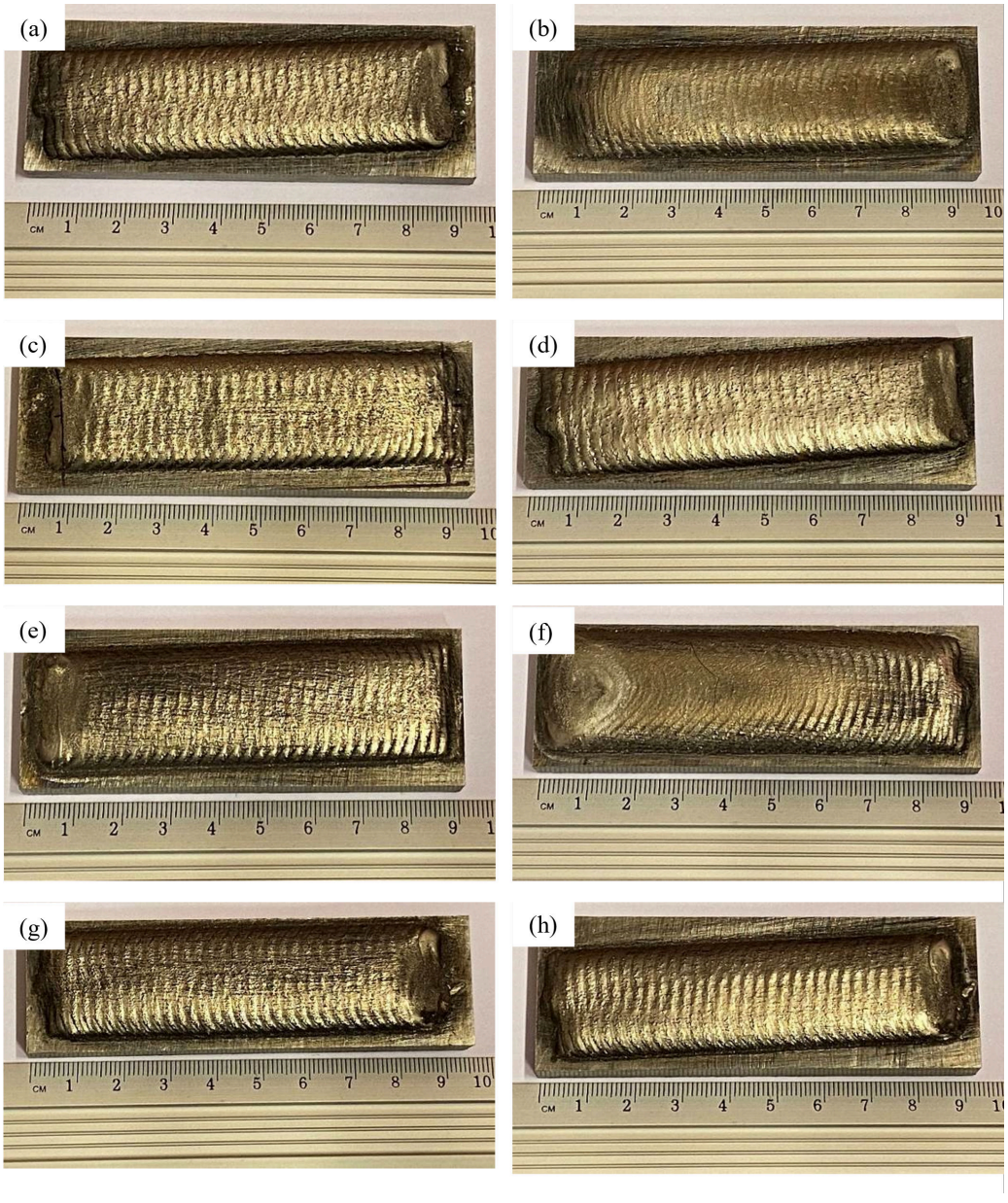

Fig. 2. Images of prepared hardfaced layers on the surface of substrate material: **(A)** PG-1, **(B)** PG-2, **(C)** PG-3, **(D)** PG-4, **(E)** PE-5, **(F)** PE-6, **(G)** PE-7, and **(H)** PE-8

hardfaced layers on the surface of the substrate material varied slightly depending on the adjustment carried out in the process parameters, and it was in the range of 2.3–3.0 mm, with the lower limit of the range characterizing largely PE-5 and the upper limit largely PG-2. This is illustrated in Figure 1B. Also, the prepared hardfaced layers on the surface of mild steel are shown in Figure 2.

2.2. Characterization and testing

Scanning electron microscopy (SEM) was performed using Supra 35 (ZEISS, Oberkochen, Germany) to obtain micrographs of the powder morphology. For metallographic investigations, for all samples, a piece of the prepared hardfaced sample was cut through a cross-section 15 mm from the end of the sample where the coating process

ended. Metallographic preparation of the specimen proceeded by grinding with SiC papers with grit sizes of 500, 800, and 1,200, polishing with a coarse diamond 130 suspension, and mirror polishing with 0.04 μm colloidal silica. Digital images of the prepared samples were captured using the Leica DVM6 digital microscope (Leica Microsystems AG, Balgach, Switzerland) to obtain information on the surface porosity and crack development. The micrographs of the microstructure of the prepared hardfaced coatings were obtained using the light microscope AxioVision (ZEISS, Jena, Germany).

A penetration test was carried out to identify cracks that had developed in the hardfaced layer after the PPTAW hardfacing process. This test was carried out based on the specifications of the PN-EN ISO 3452 standard. The test proceeded with the use of MR® 70 developer, MR® 79 remover (acetone), and MR® 68NF penetrant (MR Chemie, Unna, Germany). For each specimen, the surface was first cleaned thoroughly with acetone to eliminate impurities. The surface was then sprayed with the penetrant and allowed to dry for 10–15 min. The penetrant was then cleaned from the surface with the help of the remover and paper. The surface of the sample was then sprayed with the developer and allowed to settle for some time. After that, it would be observed that the penetrant began to appear on the surface of the specimen, from the sites where cracks existed.

The metal-mineral abrasive wear resistance test of the as-deposited hardfaced layers as well as the reference material (abrasion-resistant steel grade AR400) was carried out according to the procedures outlined in ASTM G65-00. This abrasive wear testing method, called "rubber wheel" according to the ASTM G65 standard, has been the most used test in materials engineering for assessing the metal-mineral abrasive wear resistance. Quartz sand was used in the test as the abrasive, with a grain size of 50–70 mesh (0.297–0.210 mm), and fed to the friction zone gravitationally. With regard to the PPTAW hardfaced layer and the reference material, the experimental test involved the preparation of two specimens with dimensions 75 mm × 25 mm × 10 mm. The rubber wheel made 6,000 revolutions in approximately 30 min of the test. A pressure force of 130 N was applied to the material. The feed rate of the abrasive (A.F.S. Testing Stand 50–70 mesh) was 335 g/min.

The weights of the specimens were taken before and after the abrasive wear test on the balance in the laboratory, which has an accuracy of up to 0.0001 g. The average density of the hardfaced layer and that of the reference material were determined from three measurements of the density of the specimen, sampled and weighed at room temperature in air and liquid. The volume loss was calculated from the measured average density of the hardfaced layer and the average mass loss after abrasion, using Eq. (1).

$$\text{Volume loss } \left[\text{mm}^3\right] = \frac{\text{mass loss (g)}}{\text{density } \left(\frac{\text{g}}{\text{cm}^3}\right)} \times 1{,}000 \quad (1)$$

The Archimedes method, according to the ISO ASTM D792 standard, was used to measure the density of the hardfaced layer. A Radwag AS 220.R2 analytical laboratory balance (Radwag, Warsaw, Poland) was used in the measurement along with a set for Archimedes-method-based density measurements.

The microhardness of the hardfaced layers was tested using the microhardness tester FM-ARS 9000 (Future-Tech Corp., Tokyo, Japan) to obtain the Vickers hardness with a load of 1 kg. The surface hardness was measured using a Rockwell hardness tester, SHR-1500E (Guizhou Sunpoc Tech Industry Co., Ltd., Guiyang City, China), with a load of 150 kg, to determine the effects of the different process parameters on the hardness of the prepared hardfaced layers.

3. Results

3.1. SEM visualization of powder morphology

The significance of metal matrix composites (MMCs) powders is influenced by the shape of the powder particles. Angular shaped powders are mostly preferred in wear-resistant applications, whereas spherical shaped powders are desirable in high toughness applications. A balance of these morphologies, however, results in a more mechanically balanced material that is suitable for appli-

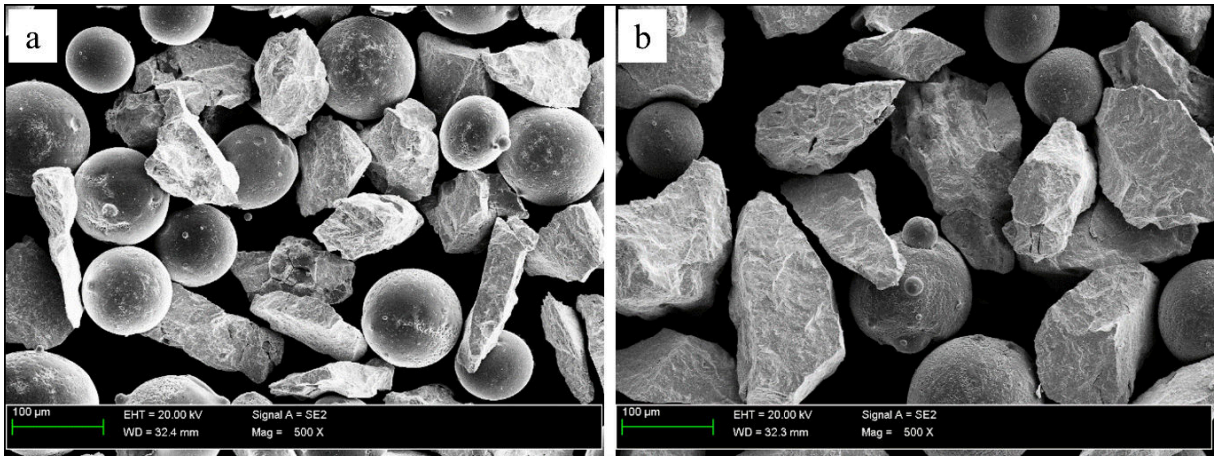

Fig. 3. SEM images of MMC powders; **(A)** PE 8214 **(B)** PG 6503. MMC, metal matrix composite; SEM, scanning electron microscopy

cations requiring high hardness, high toughness, and wear resistance [20]. The morphology of the powders used in the PPTAW process was obtained using SEM. The images obtained from this analysis are presented in Figure 3. The SEM images showed a mixed morphology of spherical and angular shaped powders (Figure 3).

3.2. Chemical composition of MMC powders

Energy dispersive X-ray spectroscopy (EDS) was used to determine the chemical composition of the MMC powders used in this study. The EDS results are presented in Figures 4 and 5 and Tables 2 and 3. This EDS investigation resulted in the observation that the powder particles were characterized by a mixed morphology: the matrix powder particles presented with spherical shapes, while the WC particles appeared with a sharp-edged angular morphology.

3.3. Microstructure of prepared samples

Considering the strong direct relationship between the structure and properties of materials, it was necessary to examine the microstructure of the prepared samples under the various conditions of preparation. The obtained micrographs, at a magnification of 500×, provided information on the dissolution of the WC particles in the Ni-based alloyed matrices under the various conditions of varying PPTAW process parameters – PGFR and PTA current. These micrographs are shown in Figure 6.

When the PGFR was increased to 1.2 l/min (Figure 6A) from 1.0 l/min (Figure 6C), the car-

Table 2. Chemical composition of PE 8214 MMC powder

Measured Point		**Ni**	**Cr**	**B**	**W**	**C**
P1	Weight%	61	5	1	30	3
	Atom%	64	6	7	10	13
P2	Weight%	42	9	2	44	3
	Atom%	45	10	13	15	17
P3	Weight%	1	-	-	96	3
	Atom%	2	-	-	69	29
P4	Weight%	4	-	-	92	3
	Atom%	9	2	-	62	27

MMC, metal matrix composite

Table 3. Chemical composition of PG 6503 MMC powder

Measured point		**Ni**	**B**	**W**	**C**
P1	Weight%	76	1	22	1
	Atom%	85	4	8	3
P2	Weight%	75	1	23	1
	Atom%	81	6	8	6
P3	Weight%	1	-	96	3
	Atom%	1	-	66	32
P4	Weight%	1	-	97	2
	Atom%	2	-	74	24

MMC, metal matrix composite

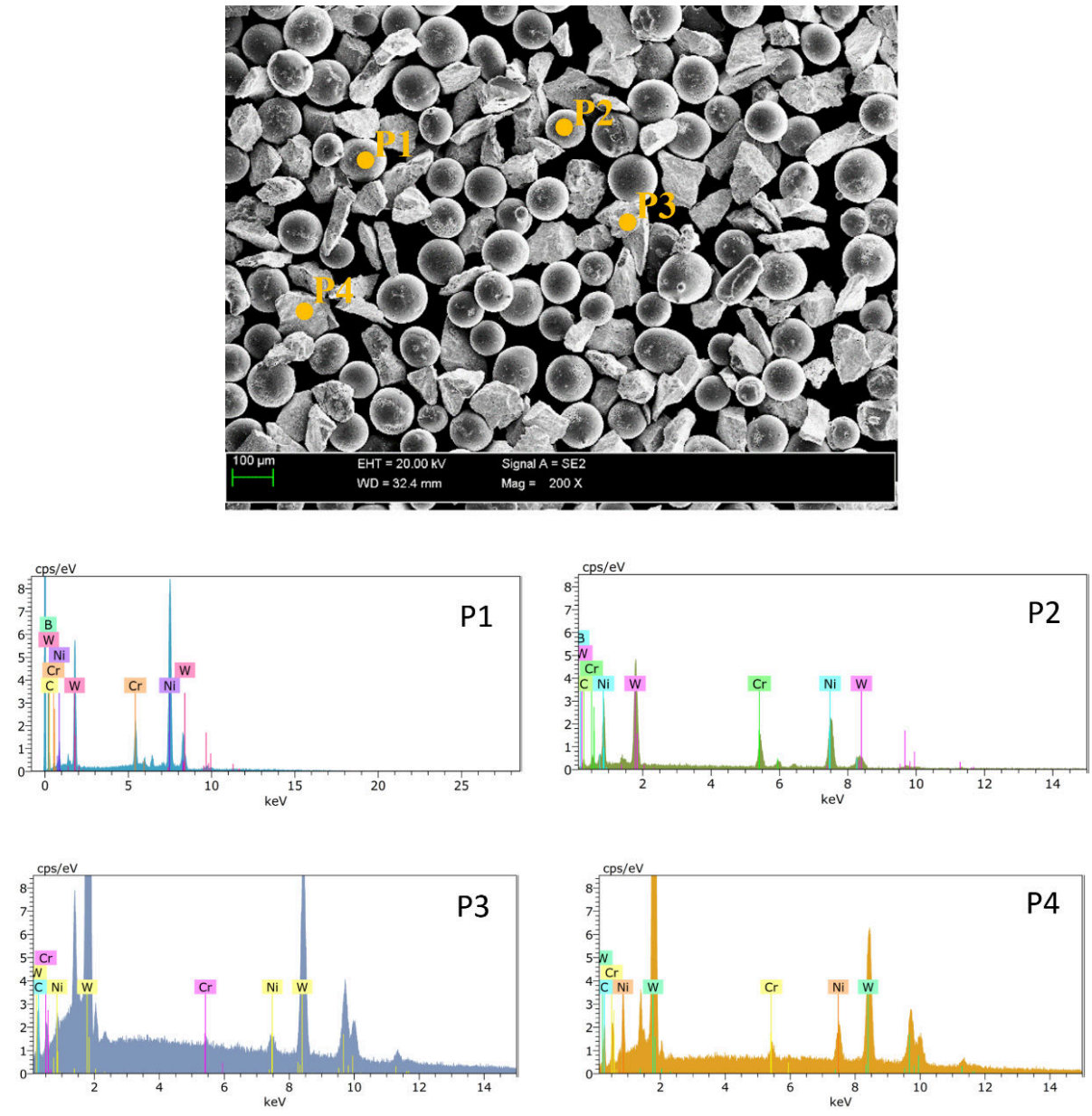

Fig. 4. EDS of powder PE 8214 showing chemical compositions. EDS, energy dispersive X-ray spectroscopy

bides were seen in the matrix with softer edges, indicating a degree of dissolution into the matrix. When the PGFR was further increased to 1.5 l/min (Figure 6D), there was still seen this same level of dissolution, as seen when the PGFR was 1.0 l/min (Figure 6C). A significant level of dissolution of the carbides into the matrix was seen when the PGFR was increased from 1.0 l/min to 1.2 l/min. However, when the PGFR was increased from 1.2 l/min to 1.5 l/min, there was no observation of a significant level of dissolution between these PGFR values. Similarly, for layers prepared with powder PE 8214, it was observed from the micrographs that the increase in the PGFR from 1.0 l/min (Figure 6G) to 1.2 l/min (Figure 6F) resulted in an observation of a slight dissolution of the carbides into the matrix. As the PGFR was increased further to 1.5 l/min (Figure 6H), there was no longer seen

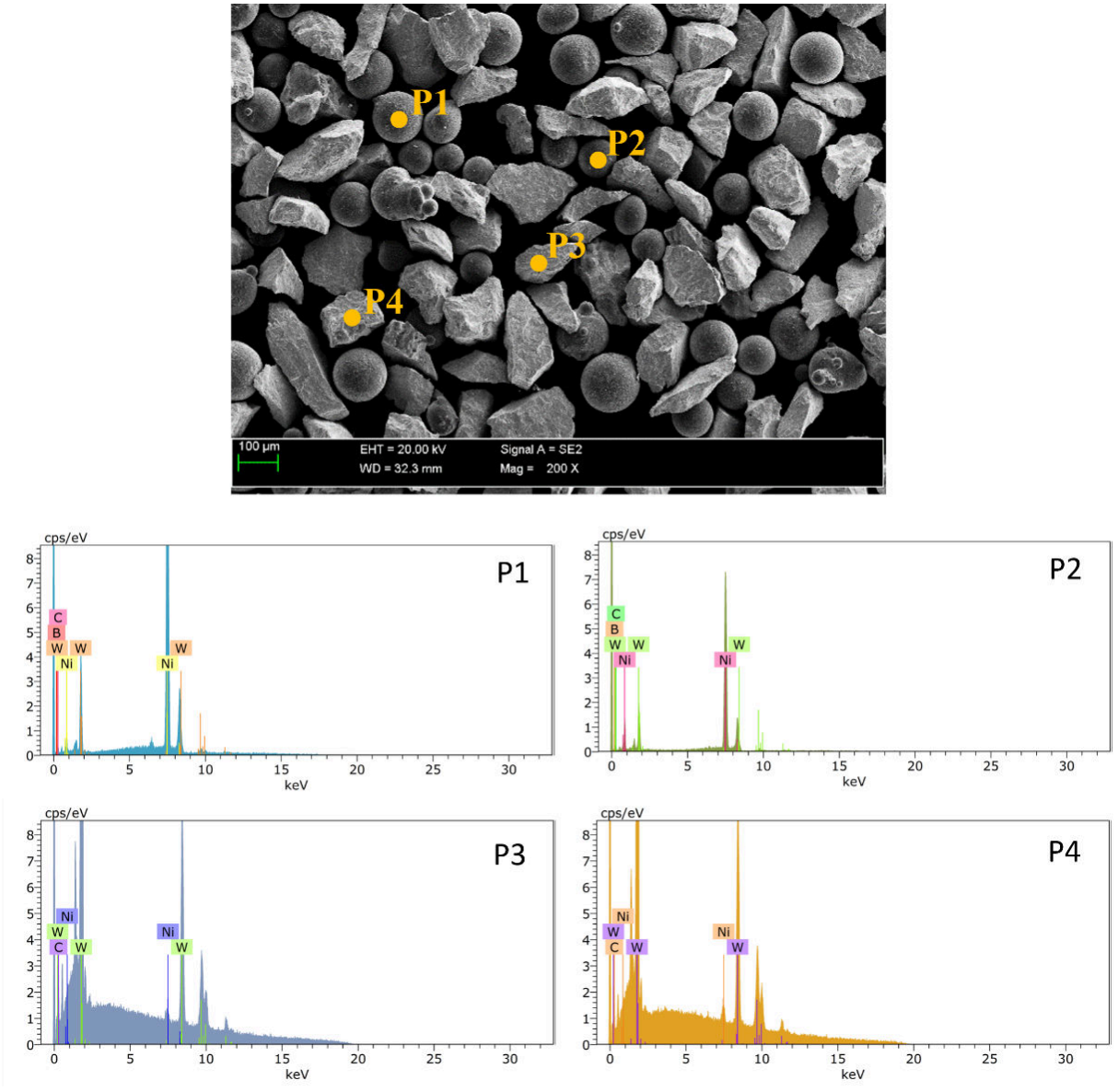

Fig. 5. EDS of powder PG 6503 showing chemical compositions. EDS, energy dispersive X-ray spectroscopy

enough dissolution of the carbides into the matrix. Generally, increasing the PGFR increased the degree of dissolution of the carbide particles into the matrix. Also, as the current was increased, the degree of dissolution of the carbides into the matrix was seen to increase slightly. Although this dissolution was not dramatic, the edges of the carbides when the current was 150 A (Figure 6B,F) were less sharp compared to when the current was 110 A (Figure 6A,E).

The microstructure of the coating observed under SEM, as displayed in Figure 7, shows the distribution of WC particles as secondary precipitates in the matrix phase. The EDS chemical maps in Figure 7B–G reveal that the gray areas in the SEM image in Figure 7A correspond to the carbides in the primary dispersed form and as precipitates in the Ni-based matrix phase, represented by the black areas in Figure 7A.

The distribution of the WC particles in the matrix phase after the hardfacing process was found to behave slightly differently for different process

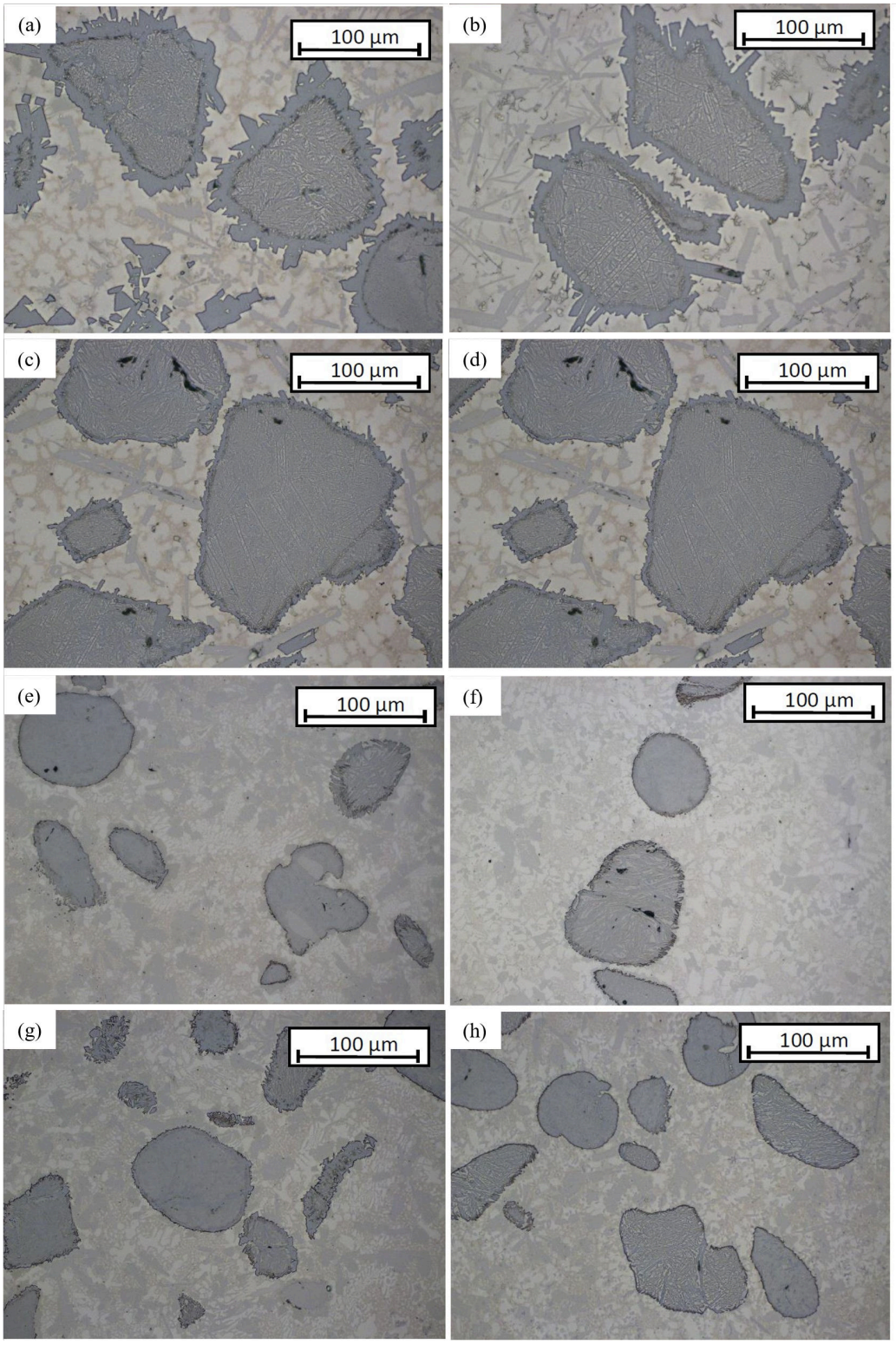

Fig. 6. Micrographs of the prepared samples at 500× magnification: **(A)** PG-1, **(B)** PG-2, **(C)** PG-3, **(D)** PG-4, **(E)** PE-5, **(F)** PE-6, **(G)** PE-7, and **(H)** PE-8

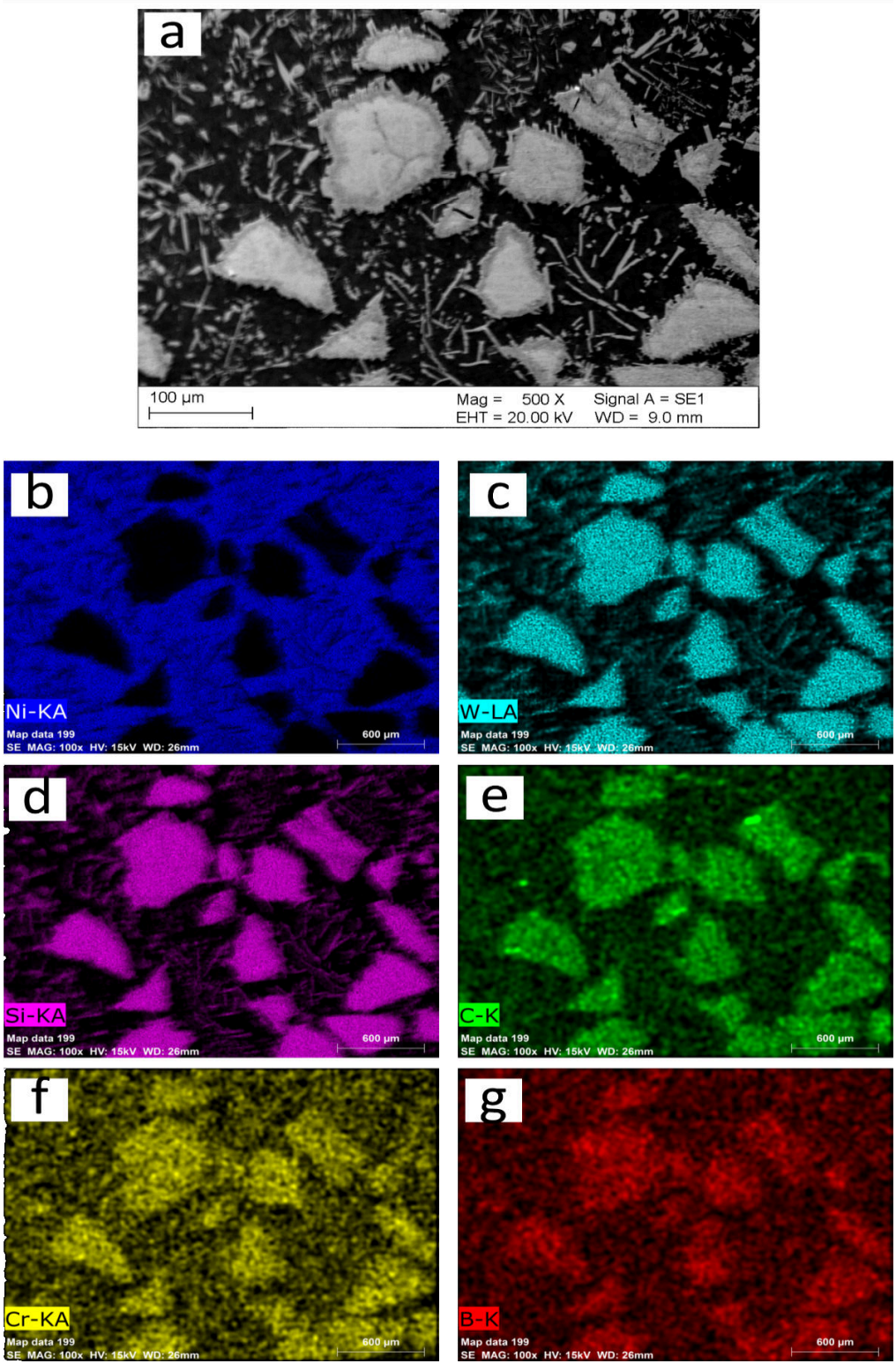

Fig. 7. EDS maps showing the chemical composition of the microstructure of the hardfaced layer **(A)** area under observation **(B–G)** elemental distribution maps. EDS, energy dispersive X-ray spectroscopy

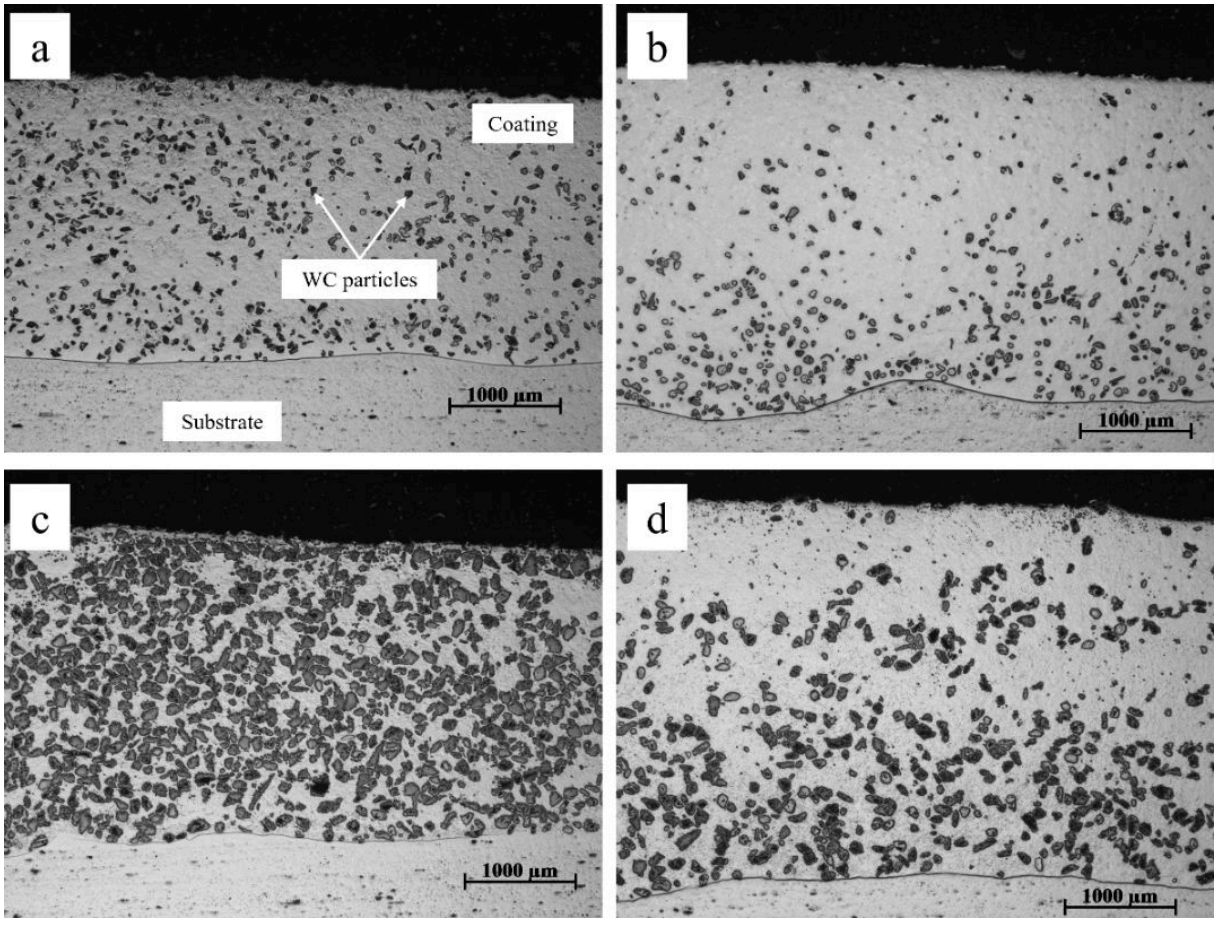

Fig. 8. Light microscopy cross-sectional image of samples showing the distribution of carbides in the Ni-based matrix under conditions of variable plasma arc current. **(A)** Sample PE-2 with PTA current of 110 A; **(B)** Sample PE-3 with PTA current of 150 A; **(C)** Sample PG-6 with PTA current of 110 A; and **(D)** Sample PG-7 with PTA current of 150 A. PTA, plasma transferred arc

parameters. It was observed that as the heat input to the hardfacing process was increased, either by increasing the PGFR or the PTA current, this observed distribution differed. To illustrate this, in Figure 8, the distributions of the carbides in the matrix have been presented for samples prepared using both MMC powders under varying conditions of PTA current. It is observed that at a lower current of 110 A, the carbides are dispersed relatively more evenly through the coating from the sub-face to the coating–substrate interface (Figures 8A and 8C). However, as the current increased to 150 A, it was observed, as shown in Figures 8B and 8D, that the WC particles were more segregated around the coating–substrate interface. A similar observation is discernable from Figure 9, which shows the effects of the variation in PTA current on the heat affected zone (HAZ). In Figures 9A and 9B, the PTA current was 110 A, and compared to the samples in Figures 9C and 9D with a PTA current of 150 A, it is seen that an increase in the PTA current correspondingly increased the HAZ. The results observed pursuant to an increase in the PGFR were similar to the observation obtained concerning the distribution of the WC particles in the matrix and the HAZ. These observations can therefore be attributed to the differences in the heat energy of the hardfacing process as the PTA current and PGFR were varied.

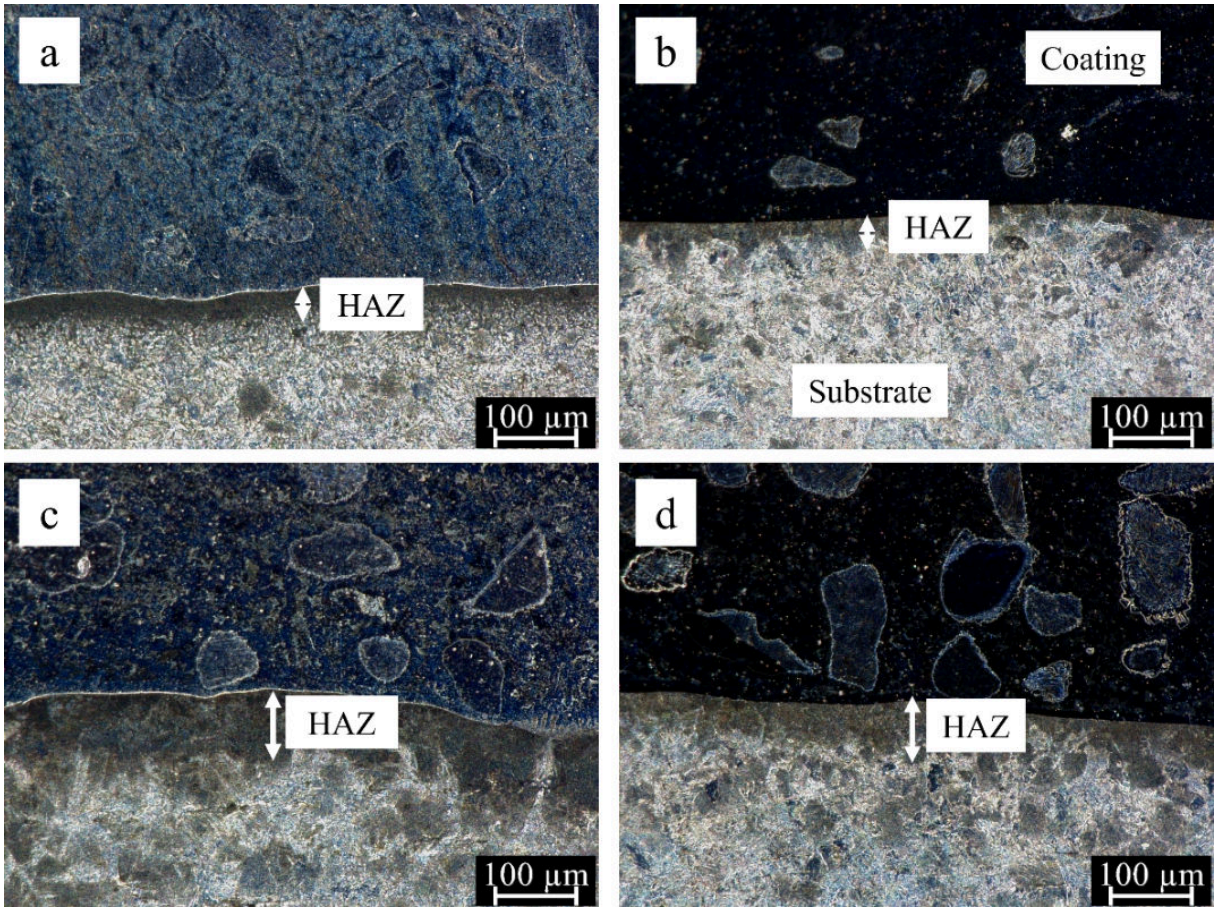

Fig. 9. Stereoscopic cross-sectional image of samples showing the HAZ under conditions of variable PTA current. **(A)** Sample PE-2 with PTA current of 110 A; **(B)** Sample PG-6 with PTA current of 110 A; **(C)** Sample PE-3 with PTA current of 150 A; and **(D)** Sample PG-7 with PTA current of 150 A. HAZ, heat affected zones; PTA, plasma transferred arc

3.4. Surface crack analyses

The formation of cracks, as well as their origin and propagation, was investigated using digital microscopy. Information regarding the depth of the cracks was also investigated in a penetration test using the guidelines outlined in the PN-EN ISO 3452 standard. Images from the digital microscopy and penetration tests are presented in Figures 10 and 11, with details on surface crack development. It was observed, both from the digital microscopy and penetration tests, that the samples prepared with the powder PE 8214 had more cracks than the samples prepared with the powder PG 6503. The penetration test results provided information on visible cracks that had been formed in the samples after preparation. As the PGFR was increased from 1.0 l/min to 1.2 l/min, there were no significant changes in the number of crack sites on the surface. However, when the PGFR was increased to 1.5 l/min, the number of crack sites was seen to increase. For all coatings prepared by both powders, there was a common observation that increasing the PPTAW current, while keeping all other parameters equal, reduced the number of crack sites in the coatings.

3.5. Abrasive wear resistance

Abrasive wear resistance tests were carried out to investigate the metal-mineral abrasive wear performance of the prepared hardfaced layers

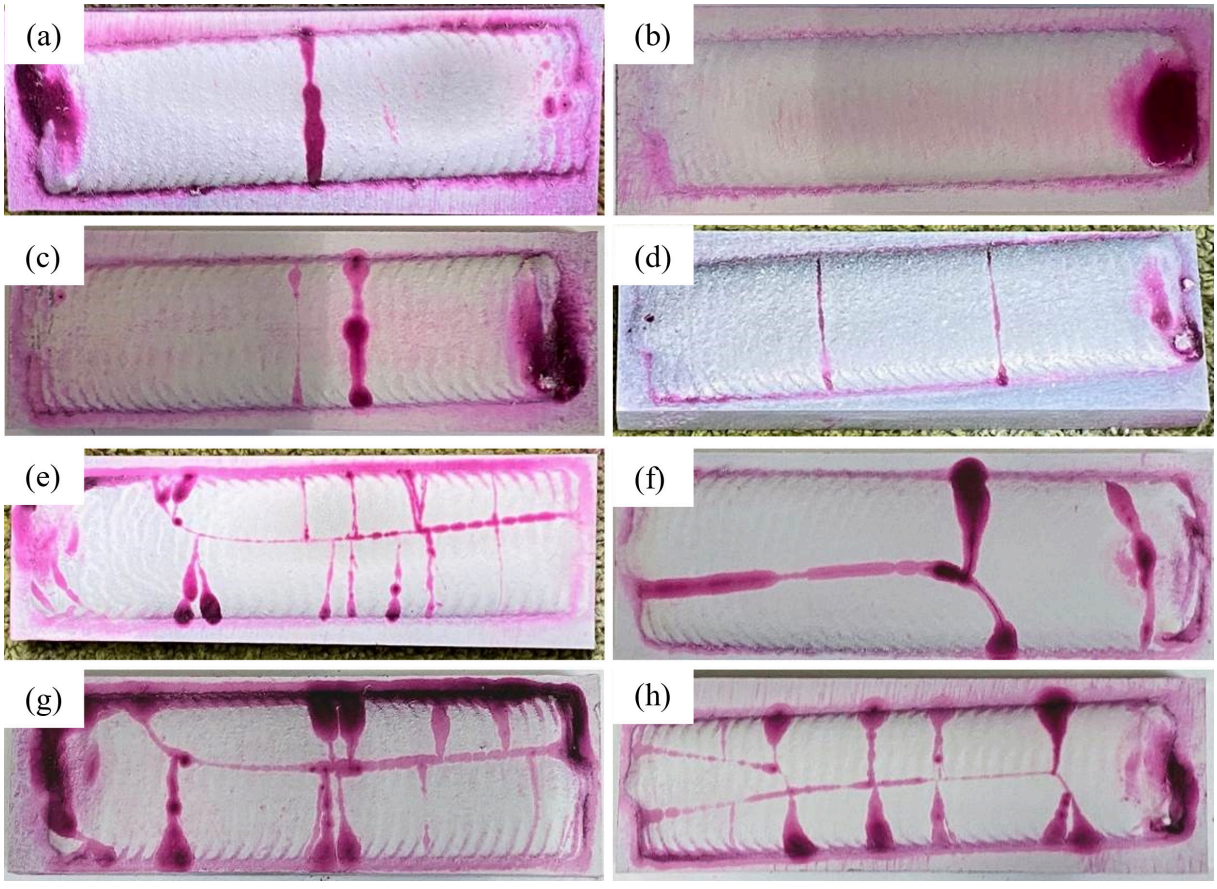

Fig. 10. Images of samples after penetration test showing the origin and depth of cracks on the surfaces of the hardfaced layers **(A)** PG-1, **(B)** PG-2, **(C)** PG-3, **(D)** PG-4, **(E)** PE-5, **(F)** PE-6, **(G)** PE-7, and **(H)** PE-8

against the abrasive resistant material Hardox 400 (AR400). The volume loss taking place as a consequence of the high difference between the density of WC and metallic matrix was estimated by using the reference material as a standard of comparison The abrasive wear resistance test results are presented in Table 4. The relative abrasive wear resistance was computed against that of the reference material, AR400. This material was selected as the reference material based on its proven resistance to abrasive wear as well as its repeated use in other research works [7, 18, 21, 22] for similar such investigations. The average volume loss and the effects of PGFR on the abrasive wear resistance of the tested samples are presented in Figure 12.

As discernible from Figure 12A, when comparing the average volume losses of the specimen with the average volume loss of the reference material, the average volume losses of the samples prepared using the powder PE 8214 were higher, with an average of 40.64 mm^3 volume loss, than the average volume losses of the samples prepared using the powder PG 6503, which had an average of 29.99 mm^3. It is seen in Figure 12B that for the samples prepared using powder PE 8214, the relative abrasive wear resistance increased with a slight increase in the PGFR but decreased as the PGFR was further increased. Conversely, for the coatings prepared using the powder PG 6503, the relative abrasive wear resistance increased as the PGFR was increased. The samples prepared with the powder PE 8214 exhibited increase in the relative abrasive wear resistance with increasing the PGFR from 1.0 l/min to 1.2 l/min, because more particles started melting into the matrix. For PE-8 that has a PGFR of 1.5 l/min, the level of porosity

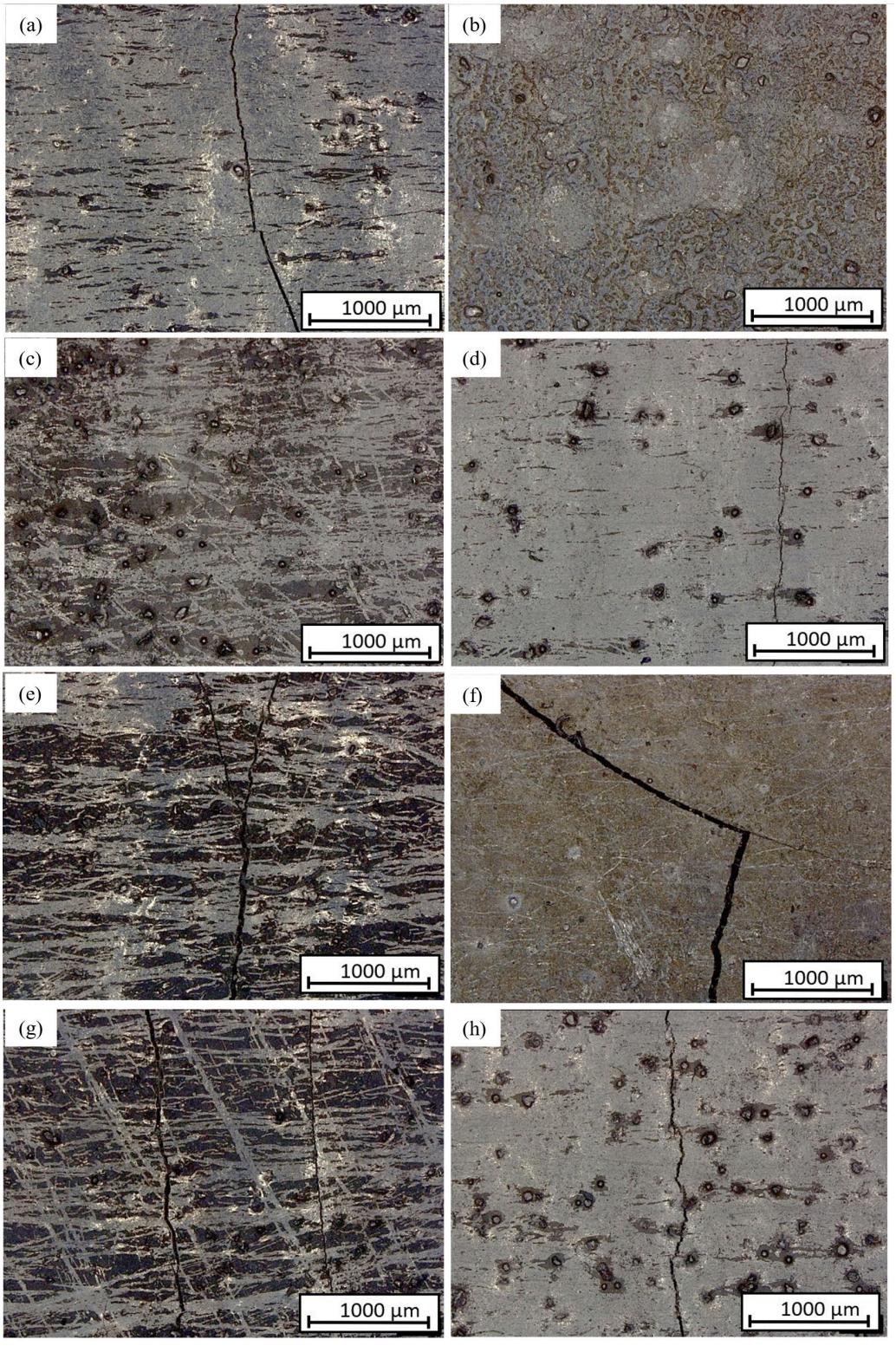

Fig. 11. Digital images of the surfaces of as-deposited hardfaced layers showing crack development and surface porosity. **(A)** PG-1, **(B)** PG-2, **(C)** PG-3, **(D)** PG-4, **(E)** PE-5, **(F)** PE-6, **(G)** PE-7, and **(H)** PE-8

Table 4. Results of the metal-mineral abrasive wear resistance tests concerning the surface layer PPTAW deposition of NiSiB + 60% WC and NiCrSiB + 45% WC composite powders on mild steel in comparison with the abrasive wear resistance of abrasion-resistant steel AR400

Sample ID	Test No.	Mass before test (g)	Mass after test (g)	Mass loss (g)	Average mass loss (g)	Material density (g/cm^3)	Average volume loss (mm^3)	Relative abrasive wear resistance*
PTAW hardfaced layer (NiSiB + 60% WC)								
PG-1	1	197.9632	197.6236	0.3396	0.3154	11.1935	28.1771	4.7
	2	193.3204	193.0292	0.2912				
PG-2	1	206.7898	206.5573	0.2325	0.2567	11.1935	22.9329	5.7
	2	211.2178	210.9369	0.2809				
PG-3	1	198.3808	197.9687	0.4121	0.3689	11.1935	32.9566	4.0
	2	193.7380	193.4123	0.3257				
PG-4	1	225.5144	225.2207	0.2937	0.3179	11.1935	28.4004	4.7
	2	230.1572	229.8151	0.3421				
PTAW hardfaced layer (NiCrSiB + 45% WC)								
PE-5	1	228.8165	228.4868	0.3297	0.3539	9.8274	36.0116	3.7
	2	224.1737	223.7956	0.3781				
PE-6	1	226.3483	226.0148	0.3335	0.3093	9.8274	31.4732	4.2
	2	230.9911	230.7060	0.2851				
PE-7	1	229.3361	228.4298	0.9063	0.7821	9.8274	79.5836	1.7
	2	233.9789	233.321	0.6579				
PE-8	1	224.0304	223.6803	0.3501	0.3742	9.8274	38.0772	3.5
	2	219.3876	218.9893	0.3983				
Reference material – AR400 steel 4								
H1		104.6219	103.4971	1.1248	1.0318	7.7836	132.5607	1.0
H2		111.7377	110.7989	0.9388				

*Relative abrasive wear resistance is in relation to the abrasion-resistant steel AR400.
PPTAW, powder plasma transferred arc welding; PTAW, plasma transferred arc welding

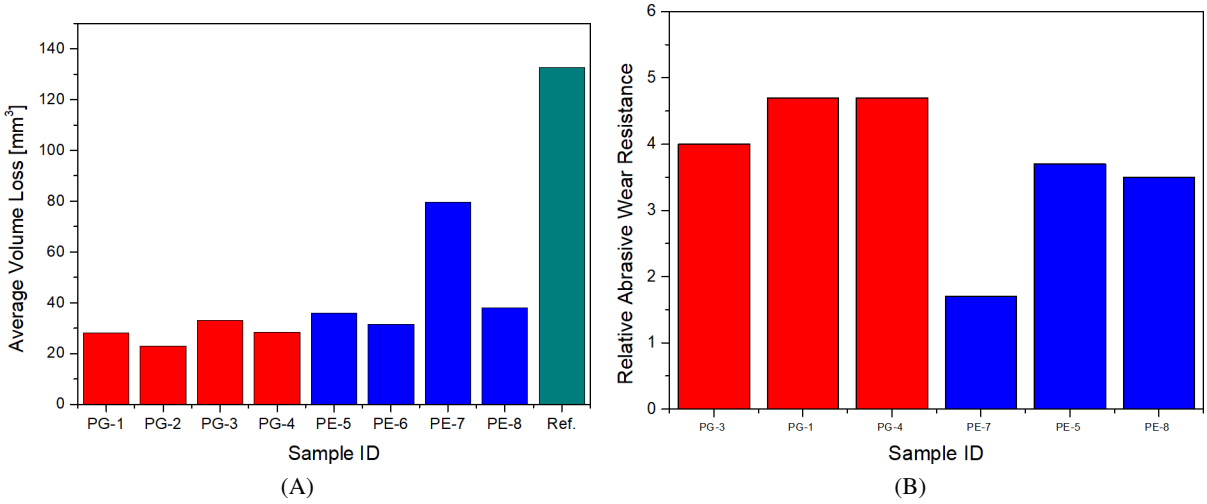

Fig. 12. **(A)** Graphs showing how the average volume losses of the specimen compare with the average volume loss of the reference material; **(B)** Relative abrasive wear resistance with changes in PGFR

Table 5. Microhardness across the cross-section of hardfaced layers

Sample ID	Microhardness of matrix, HV		Microhardness of carbides, HV	
	Mean	Standard deviation	Mean	Standard deviation
PG-1	591	5.2	2,413	62.9
PG-2	573	10.2	2,129	33.3
PG-3	687	2.4	2,163	76.1
PG-4	673	18.5	2,275	49.5
PE-5	889	18.0	2,349	38.7
PE-6	845	23.2	2,436	24.1
PE-7	889	23.8	2,343	61.6
PE-8	893	16.1	2,391	80.5

in the coating was lower, which resulted in a higher relative abrasive wear resistance. The calculations of relative abrasive wear resistance in Table 4 indicate that, in the case of the coatings prepared with the powder PG 6503, the relative abrasive wear resistance significantly reduced as the current was increased from 110 A in PG-1 to 150 A in PG-3. Similarly, there was a reduction in the relative abrasive wear resistance in the coatings prepared with the powder PE 8214 when the current was increased from 110 A in PE-5 to 150 A in PE-7. The layers prepared with the powders of PG 6503 exhibited higher relative abrasive wear resistance than those prepared with the powders of PE 8214.

3.6. Hardness

The surface hardness was tested for the hardfacings to investigate the contributions of the various process parameters to the hardness of the surface. The microhardness of the matrix and carbides were determined by measuring the hardness at random points in the cross-section of the coating and reporting the average of 10 measured points. The surface hardness was measured along the surface of the coating with a total of eight points, with 5 mm between each point. Table 3 shows the microhardness results for both the matrix and the carbides for the layers based on both powders. The results of the Rockwell C surface hardness test are presented in Table 4.

It is observed from Tables 5 and 6 that the hardness values of the samples prepared by the powder PE 8214 (NiCrSiB + 45% WC) were greater than the values of the samples prepared by the powder

Table 6. Surface hardness of hardfaced layers

Specimen	Rockwell hardness (HRC)	
	Mean	Standard deviation
PG-1	46.3	0.5
PG-2	47.3	2.6
PG-3	47.7	2.5
PG-4	48.3	1.2
PE-5	58.3	3.7
PE-6	52.7	3.3
PE-7	55.3	2.9
PE-8	55.7	1.2

PG 6503 (NiSiB + 60% WC), from the surfaces of the coatings and even at the interfaces. However, the values were the same in the substrate material. This observation of higher hardness in PE 8214 than PG 6503 can be explained by the presence of chromium in the powder PE 8214. Tian et al. [23] investigated the effect of chromium content on the mechanical properties of an alloy. Findings from their study reported that increasing the chromium content in the alloy significantly increased the hardness and the wear resistance.

4. Discussion

4.1. Dilution

The powder feeder used in this study is designed and intended for applications that enable feeding of different powders to the weld pool consisting of the Ni-based matrix and the carbides. A programmable logic controller (PLC) was used to control the rate of feeding. The plasma, shielding, and carrier gases were used to perform the coaxial

Table 7. Geometrical properties and dilution ratio of prepared hardfaced layers

Sample ID	Layer height, R (mm)	Penetration depth, P (mm)	Layer width, w (mm)	Dilution, D (%)
PG-1	2.9	0.2	23	1.1
PG-2	2.7	0.5	24	4.5
PG-3	1.7	0.3	23	3.7
PG-4	2.2	0.4	24	4.3
PE-5	2.2	0.2	24	0.9
PE-6	2.6	0.4	23	2.1
PE-7	2.8	1.4	25	7.8
PE-8	3.0	1.0	25	6.6

injection of the powder. To determine an ideal combination of parameters that would yield the most desirable properties, formation of the weave-bead hardfacings was studied under the prevalence of two variant values of the plasma arc current, at 110 A and 150 A, together with three variant values of the PGFR, at 1.0 l/min, 1.2 l/min, and 1.5 l/min, as demonstrated in Figure 2. Figure 13 shows the area of dilution with dilution ratio, D, influenced by the PPTAW process parameters and calculated using Eq. (2).

$$\text{Dilution, D} = \frac{Fw}{Fw+Fn} \times 100 \qquad (2)$$

where Fn is the area of the hardfaced layer on the substrate, called the reinforcement area, and Fw is the fusion zone area. The geometrical schematic shown in Figure 13 also shows the height of the hardfaced layer on the substrate material (R), the penetration depth of the hardfaced layer into the substrate (P), and the width of the hardfaced layer across the x-plane (w).

Table 7 gives the values of the measured geometrical parameters and the computed values of D for the tested samples. The values of D were the lowest (1.1% for PG-1 and 0.9% PE-5) when the PTA current was the lowest at 110 A and PGFR was also at the lowest at 1.0 l/min. However, at higher PTA current and PGFR for samples PG-4 and PE-7, the dilution ratio was seen to be relatively higher. Relative to other surface cladding technologies like metal arc welding, gas tungsten arc welding, gas metal arc welding, etc., which have dilution ratios ranging between 10% and 30%, PTA welding usually proceeds with a lower dilution, typically

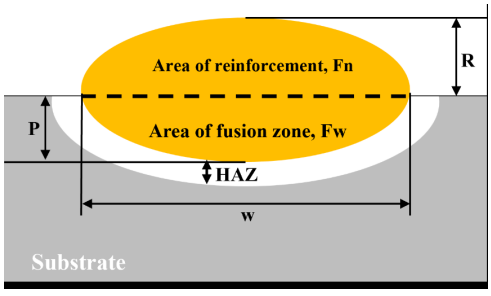

Fig. 13. Schematic of the geometrical parameters of the cross-section of the final material after deposition of the hardfaced layer onto the substrate material, showing the reinforcement area, fusion zone area, and HAZ. HAZ, heat affected zone

<10%, as reported in the studies of Czupryński [22] and Lakshminarayanan et al. [24].

4.2. Effect of MMC powder particle morphology

The selection of the wear-resistant powders used in this study was aimed at the morphological structure of the powder particles, as well as the effects of this morphology on the wear resistance of the produced hardfaced layers. The conducted SEM analysis (Figure 3) revealed that the powders used had a mixed morphology of spherical and angular shapes. In a study on the effects of WC powder particle morphology on the wear rate of surface coatings, Huang et al. [25] reported that the wear resistance of the coating layer is influenced by a mean free distance that exists between WC particles, where even the slightest dissolution of the WC particles would have significant effects on the wear properties of the coating. This was observed

because the hardfaced layers formed by spherical powder particles showed wider gaps between the reinforcement, which contrasts with the interlocking nature of the structure formed by the angular powder particles, reducing the contact between the abrasive particle and the matrix material [25]. This observation finds substantiation in the present study; as less WC particles were dissolved in PG-3 (Figure 6C) than in PG-4 (Figure 6D), it can accordingly be inferred that the relative abrasive wear resistance increased corresponding to the transition of the material used from PG-3 to PG-4, as reported in Table 4.

4.3. Effects of PGFR on the mechanical properties of the hardfaced layers

The current state of PPTAW provides insight into how PGFR is a major contributing factor to the resultant mechanical properties of the hardfaced layer [21, 26]. The present research studies the effects of PGFR on the hardfaced layers' microstructure, hardness, abrasive wear resistance, and crack formation and propagation. An increase in the PGFR had a corresponding increase in the rate of dissolution of the particulate carbides into the matrix. This increase, however, was seen to be not significant as the PGFR values increased further. This observation can be explained by the presence of residual plasma gas in the plasma jet when the PGFR was high. This inhibited progressive heat dissipation and consequently prevented further dissolution of powder particles [27].

There was a direct relationship between the values of PGFR and the number of crack sites present in the hardfaced layer, for layers prepared from both powders. At higher values of PGFR, there was increased pore formation resulting from plasma gas that had been entrapped in the plasma jet. This entrapment resulted in inadequate melting of particles that had agglomerated and hence they exhibited low thermal conductivity, resulting in poor resistance to crack formation by the hardfaced layers.

The abrasive wear resistance exhibited by the layers prepared with the powder with composition NiCrSiB + 45% WC (PE 8214) was lower than that exhibited by the layers prepared with the powder NiSiB + 60% WC (PG 6504). The difference in the relative abrasive wear resistance as observed was not statistically big, even though the powder with a high content of WC exhibited high abrasive wear resistance. This observation was particularly noticeable as the PGFR was increased in both situations and it could be attributed to the presence of chromium in the PE 8214 powders. Alloying with Cr increases the wear resistance of materials [23]. El-Mahallawi et al. [28] evaluated the effect of Cr in alloys by studying high manganese steel containing 1–7 wt.% and 2–3 wt.% Cr. These steels were subjected to various wear conditions including abrasion, corrosion, and combined impact-abrasive wear. The performance of these Cr alloyed steels was compared to those observed with plain Hadfield steels, and it was reported that the Cr alloyed manganese steels had wear resistance superior to those of the Hadfield steels. This also supported the observation of an increase in the abrasive wear resistance as the PGFR was increased for samples prepared with this powder. The PGFR aided in introducing powder materials onto the surface of the substrate, and as it increased, more powders were deposited in the PPTAW process [27]. This resulted in an increase in the Cr content in the hardfaced layer, with a corresponding increase in wear resistance. A similar outcome was observed in the study by Tian et al. [23] on the effect of chromium content on microstructure, hardness, and wear resistance of as-cast Fe-Cr-B alloy. The Cr content was varied from 0 wt.%, in increments of 4 wt.% to 20 wt.%. It was observed that as the Cr content increased, the wear resistance and hardness also increased until reaching an equilibrium at 12 wt.% Cr, after which there was not much of a significant increase in these mechanical properties.

Hardfaced layers prepared by both powders exhibited an increase in hardness when the PGFR was also increased. As the PGFR was increased, the plasma power correspondingly increased, resulting in a higher particle temperature. With an increased temperature of the particles, dissolution of the carbides into the matrix was accelerated. This enhanced the adhesion between the particles, resulting in lower porosity and enhanced hardness [29].

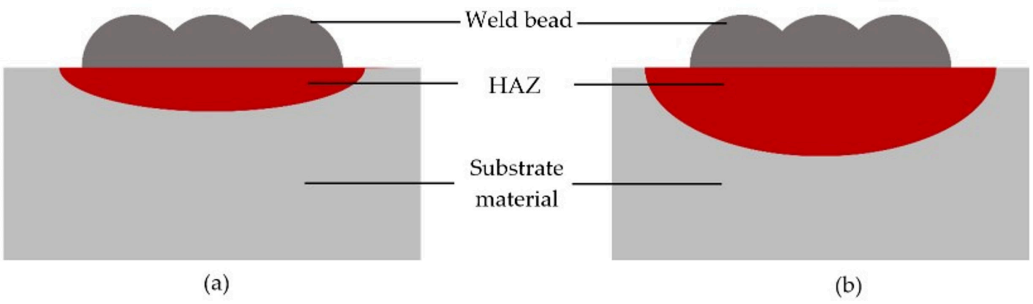

Fig. 14. Comparison of HAZ with an increase in PTA current. **(A)** The HAZ is smaller with a lower value of PTA current at 110 A; **(B)** The HAZ is larger with an increased value of PTA current at 150 A. HAZ, heat affected zones; PTA, plasma transferred arc

4.4. Effects of PTA current on the mechanical properties of the hardfaced layers

Increasing the PPTAW process current resulted in higher degrees of dissolution of the carbides into the matrix, with corresponding reduction in crack formation, as well as the number of crack sites in the layered coatings. The surfaces of the coatings obtained pursuant to an increased PTA current tend to be characterized by greater smoothness and fewer cracks. This was because as the current increased, the particles absorbed more energy, creating a rise in particle temperature, resulting in the eventual reduction in porosity of the system [20]. The state of stress in the padding weld was also affected by the amount of heat introduced into the material. The greater the amount of the supplied heat, the slower the rate of dissipation of heat from the material into the environment, resulting in a lower stress state and an eventual reduction in cracks [30]

A rise in the plasma arc current mostly resulted in an increase in the fraction of the base material in the padding weld, resulting in an increase in wear resistance [22]. In this work, however, for both powders, the coatings formed had a reduction in the relative abrasive wear resistance when the current was increased from 110 A to 150 A. This is because it was observed that an increase in the PTA current increased the dissolution of the powder particles. This caused the surface to be smoother with shallow grooves on the surface, as shown in samples PG-3 (Figure 2C) and PG-4 (Figure 2D). These smoother surface and shallow surface grooves contribute to the reduction in the relative abrasive wear resistance of the coatings [31]. Adjusting the PTA current to a higher value provided more energy for absorption by the powder particles, causing an increase in temperature. This resulted in reduction in porosity, as the rate of dissolution of the powder particles increased with increasing PTA current. The higher rate of particle dissolution and lower levels of porosity associated with an increase in the PTA current resulted in the increase in the hardness of the coatings [32]. This was indicative of the higher microhardness values recorded in this study as the PTA current was increased. It is reported in Tables 5 and 6 that as the PTA current was increased, there was a corresponding increase in the surface hardness as well as the depth of the microhardness across the cross-section of the layers. This was because the depth of the HAZ increased as the PTA current increased since there was a rise in the output heat of the plasma in this situation. Comparison of the size of the HAZ with increase in PTA is given in Figure 9 and visualized in Figure 14. Higher hardness is desirable in some applications; however, due to the growth of the HAZ as the PTA current is increased, producing the hardfaced layers at higher PTA current intensities is not encouraged. This is because the introduced heat results in a more brittle microstructure upon cooling, and this will significantly affect the toughness of the material and result in poor adhesion at the substrate-coating interface [33].

4.5. Abrasive wear mechanism

The abrasive wear resistance tests performed on the prepared hardfaced layers proceeded in conformity with the procedures outlined in ASTM G65-00. A rubber wheel with quartz sand of grain size 0.297–0.210 mm was used for this test. Initially, there was removal of tiny amounts of wear debris from the surface as the rubber wheel and quartz sand got into contact with the surface. At this stage, the bulk of the WC particles were positioned slightly below the surface. The surface was mostly composed of the Ni-based matrix. Revolutions from the rubber wheel propelled the quartz sand to remove material from the surface as the wear phenomenon gradually approached the mass of the WC particles. As the quartz sand eventually got into contact with the WC particles, it gradually smeared and began to wear off the carbides. As the operation proceeded, WC particles previously at the subsurface of the hardfaced layer got exposed onto the surface of the layer. This film reduced the friction from the quartz sand and eventually reduced the wear rate significantly. The position of the bulk of the WC particles away from the surface of the layer depended on the values of PGFR and PTA current. These parameters increase the heat of the system as they increase, causing more melting of the powder particles on the surface. With an increase in the PTA current, the surface of the layer becomes smoother, facilitating the wear rates of the quartz sand on the surface [34].

5. Conclusions

1. PPTAW technology was used to prepare hardfaced layers on the surface of a mild steel plate based on the powders of wear-resistant Ni-based matrix with WC reinforced metal matrix composites (MMCs) of composition NiCrSiB + 45% WC and NiSiB + 60% WC. Relative to wear-resistant steel Hardox 400, the wear resistance of the prepared layers was significantly higher. The introduction of Cr as an alloying element contributed to increasing the hardness and wear resistance of the layers. Coatings were prepared by varying the PPTAW process parameters – the variations employed were PGFR at 1.0 l/min, 1.2 l/min, and 1.5 l/min; and plasma arc current at 110 A and 150 A.
2. Adjustment of the PGFR to slightly higher values had a corresponding increase in the rate of dissolution of the WC particles in the Ni-based matrix, in its microstructure. This resulted in an increase in the hardness of the hardfaced layer, as well as increase in the abrasive wear resistance. However, at higher values of PGFR, there is development of more cracks on the surface of the layers.
3. Increasing the PTA current also increased the amount of heat introduced and absorbed by the particles, creating a larger HAZ. The hardness of the hardfaced layer was observed to increase; however, this increase in PTA current resulted in a reduction in wear resistance. The higher heat accompanying the increased current resulted in a greater dissolution of the WC particles into the Ni-based matrix, revealing a much smoother surface with fewer cracks.

Acknowledgements

The authors would like to express their gratitude to Castolin Sp. z o.o., Leonarda da Vinci 5 Str., 44-109 Gliwice, Poland for technical support in test samples' preparation.

Funding

This research was partially funded by the Silesian University of Technology under Program "Inicjatywa Doskonałości – Uczelnia Badawcza", grant No. 31/010/SDU20/0006-10.

References

[1] Fotovvati B, Namdari N, Dehghanghadikolaei A. On coating techniques for surface protection: a review. J Manuf Mater Process. 2019;3(1):28.

[2] Ashby MF, Jones DR. Engineering materials 1: an introduction to properties, applications and design. Pergamon Press,Oxford; Vol. 1: Elsevier; 2011.

[3] Kern W, Schuegraf KK. Deposition technologies and applications: introduction and overview. In: Handbook of thin film deposition processes and techniques: William Andrew Publishing; Elsevier; 2001. pp. 11–43.

[4] Kołodziejczak P, Golański D, Chmielewski T, Chmielewski M. Microstructure of rhenium doped Ni-Cr deposits produced by laser cladding. Materials. 2021;14(11):2745.

[5] Kołodziejczak P, Bober M, Chmielewski T. Wear resistance comparison research of high-alloy protective coatings for power industry prepared by means of CMT cladding. Appl Sci. 2022;12(9):4568.
[6] Górka J, Czupryński A, Żuk M, Adamiak M, Kopyść A. Properties and structure of deposited nanocrystalline coatings in relation to selected construction materials resistant to abrasive wear. Materials. 2018;11(7):1184.
[7] Górka J, Czupryński A, Adamiak M. Properties and structure of nanocrystalline layers obtained by manual metal arc welding (MMA). Arch Metall Mater. 2017;62;1479-1484
[8] Branagan D, Marshall M, Meacham B. High toughness high hardness iron based PTAW weld materials. Mater Sci Eng A. 2006;428(1–2):116–23.
[9] Veinthal R, Sergejev F, Zikin A, Tarbe R, Hornung J. Abrasive impact wear and surface fatigue wear behaviour of Fe–Cr–C PTA overlays. Wear. 2013;301(1–2):102–8.
[10] Rohan P, Boxanova M, Zhang L, Kramar T, Lukac F. High speed steel deposited by pulsed PTA-Frequency influence. ASM International 2017; In ITSC2017; pp 404-407.
[11] Zikin A, Hussainova I, Katsich C, Badisch E, Tomastik C. Advanced chromium carbide-based hardfacings. Surf Coat Technol. 2012;206(19–20):4270–8.
[12] Skowrońska B, Sokołowski W, Rostamian R. Structural investigation of the plasma transferred arc hardfaced glass mold after operation. Weld Technol Rev. 2020;92(3):55–65.
[13] Bober M, Senkara J. Comparative tests of plasma-surfaced nickel layers with chromium and titanium carbides. Weld Int. 2016;30(2):107–11.
[14] Niu J, Guo W, Guo M, Lu S. Plasma application in thermal processing of materials. Vacuum. 2002;65(3–4):263–6.
[15] Mendez PF, Barnes N, Bell K, Borle SD, Gajapathi SS, Guest SD, et al. Welding processes for wear resistant overlays. J Manuf Process. 2014;16(1):4–25.
[16] Kesavan D, Kamaraj M. The microstructure and high temperature wear performance of a nickel base hardfaced coating. Surf Coat Technol. 2010;204(24):4034–43.
[17] Szala M, Hejwowski T, Lenart I. Cavitation erosion resistance of Ni-Co based coatings. Adv Sci Technol Res J. 2014;8(21):36–42.
[18] Appiah ANS, Bialas O, Czupryński A, Adamiak M. Powder plasma transferred arc welding of Ni-Si-B+ 60 wt% WC and Ni-Cr-Si-B+ 45 wt% WC for surface cladding of structural steel. Materials. 2022;15(14):4956.
[19] Mandal S, Kumar S, Bhargava P, Premsingh C, Paul C, Kukreja L. An experimental investigation and analysis of PTAW process. Mater Manuf Process. 2015;30(9):1131–7.
[20] Qi C, Zhan X, Gao Q, Liu L, Song Y, Li Y. The influence of the pre-placed powder layers on the morphology, microscopic characteristics and microhardness of Ti-6Al-4V/WC MMC coatings during laser cladding. Opt Laser Technol. 2019;119:105572.
[21] Czupryński A, Żuk M. Matrix composite coatings deposited on AISI 4715 steel by powder plasma-transferred arc welding. Part 3. Comparison of the brittle fracture resistance of wear-resistant composite layers surfaced using the PPTAW method. Materials. 2021;14(20):6066.
[22] Czupryński A. Microstructure and abrasive wear resistance of metal matrix composite coatings deposited on steel grade AISI 4715 by powder plasma transferred arc welding part 1. Mechanical and structural properties of a cobalt-based alloy surface layer reinforced with particles of titanium carbide and synthetic metal–diamond composite. Materials. 2021;14(9):2382.
[23] Tian Y, Ju J, Fu H, Ma S, Lin J, Lei Y. Effect of chromium content on microstructure, hardness, and wear resistance of as-cast Fe-Cr-B alloy. J Mater Eng Perform. 2019;28(10):6428–37.
[24] Lakshminarayanan AK, Balasubramanian V, Varahamoorthy R, Babu S. Predicting the dilution of plasma transferred arc hardfacing of stellite on carbon steel using response surface methodology. Met Mater Int. 2008;14(6):779.
[25] Huang S, Samandi M, Brandt M. Abrasive wear performance and microstructure of laser clad WC/Ni layers. Wear. 2004;256(11–12):1095–105.
[26] Xu H, Huang H, Liu Z. Influence of plasma transferred arc remelting on microstructure and properties of PTAW-deposited Ni-based overlay coating. J Therm Spray Technol. 2021;30(4):946–58.
[27] Li GL, Ma JL, Wang HD, Kang JJ, Xu BS. Effects of argon gas flow rate on the microstructure and micromechanical properties of supersonic plasma sprayed nanostructured Al2O3-13 wt.% TiO2 coatings. Appl Surf Sci. 2014;311:124–30.
[28] El-Mahallawi I, Abdel-Karim R, Naguib A. Evaluation of effect of chromium on wear performance of high manganese steel. Mater Sci Technol. 2001;17(11):1385–90.
[29] Wilden J, Bergmann J, Frank H. Plasma transferred arc welding—modeling and experimental optimization. J Therm Spray Technol. 2006;15(4):779–84.
[30] Xiong Y, Lin D, Zheng Z, Li J, Deng T. The effect of different arc currents on the microstructure and tribological behaviors of Cu particle composite coating synthesized on GCr15 steel by PTA surface alloying. Metals. 2018;8(12):984.
[31] Fernandes F, Lopes B, Cavaleiro A, Ramalho A, Loureiro A. Effect of arc current on microstructure and wear characteristics of a Ni-based coating deposited by PTA on gray cast iron. Surf Coat Technol. 2011;205(16):4094–106.
[32] Paes R, Scheid A. Effect of deposition current on microstructure and properties of CoCrWC alloy PTA coatings. Soldag Insp. 2014;19:247–54.

[33] Om H, Pandey S. Effect of heat input on dilution and heat affected zone in submerged arc welding process. Sadhana. 2013;38(6):1369–91.

[34] Bansal A, Zafar S, Sharma AK. Microstructure and abrasive wear performance of Ni-WC composite microwave clad. J Mater Eng Perform. 2015;24(10):3708–16.

Received 2022-10-24
Accepted 2022-11-11